Redox-dependent Structure and Dynamics of Macrophage Migration Inhibitory Factor Reveal Sites of Latent Allostery

Erin Skeens,[1] Meagan Gadzuk-Shea,[2] Dilip Shah,[3] Vineet Bhandari,[3] Devin K. Schweppe,[2] Rebecca B. Berlow,[4]* and George P. Lisi[1]*

[1]Department of Molecular Biology, Cell Biology, & Biochemistry, Brown University, Providence, RI 02903
[2]Department of Genome Sciences, University of Washington, Seattle, WA 98195
[3]Section of Neonatology, Department of Pediatrics, Cooper University Hospital, Camden, NJ 08103
[4]Department of Integrative Structural and Computational Biology, The Scripps Research Institute, La Jolla, CA 92037

*To whom correspondence should be addressed: George P. Lisi (george_lisi@brown.edu)
Rebecca B. Berlow (rberlow@scripps.edu)

ORCID: Erin Skeens (0000-0002-0580-1291)
Rebecca B. Berlow (0000-0003-1934-0139)
George P. Lisi (0000-0001-8878-5655)
Meagan Gadzuk-Shea (0000-0001-9496-529X)

Abstract

Macrophage migration inhibitory factor (MIF) is a multifunctional immunoregulatory protein that is a key player in the innate immune response. Given its overexpression at sites of inflammation in a wide range of diseases marked by increasingly oxidative cellular environment, a comprehensive structural understanding of how cellular redox conditions may impact the structure and function of MIF is necessary. We used solution NMR spectroscopy and mass spectrometry to investigate structural and dynamic signatures of MIF under varied solution redox conditions. Our results indicate that the MIF structure is modified and becomes increasingly dynamic in an oxidative environment, which may be a means to alter the MIF functional response in a redox-dependent manner. We identified latent allosteric sites within MIF that are redox-sensitive and mutational analysis reveals that loss of redox-responsive residues attenuates activation of the coreceptor CD74. Leveraging sites of redox-sensitivity therefore reveals an avenue to modulate MIF function in its "disease state" via structure-based drug design.

Introduction

Macrophage migration inhibitory factor (MIF) is a ubiquitous human protein that plays a crucial role in the pathophysiology of inflammation.[1] MIF is expressed by nearly every cell in the body[1] and many of its effects are elicited by its binding to the chemokine receptors CXCR2 and CXCR4[2,3] or the coreceptor CD74.[4-6] Circulating levels are reported in the low μM range in healthy humans,[7-9] but MIF is overexpressed under inflammatory conditions and has been linked to glucocorticoid overriding activity,[10] asthma,[7,11] rheumatoid arthritis,[12] colitis,[13] pancreatitis,[14] acute respiratory distress syndrome (ARDS),[15] and cancer[16-20] as well as complications from COVID-19.[21] Efforts to elucidate the pathogenic mechanism of MIF have attempted to connect

24 its disease state to cellular redox properties,[11] most recently by investigating its cysteine
25 residues as conformational switches.[22] Mutation of either C56 or C59 in a canonical ^{56}CXXC^{59}
26 (XX = AL in MIF) motif modulates the enzymatic and macrophage activation functions of MIF.[23,24]
27 An oxidative cellular environment is one of the hallmarks of inflammatory disease,
28 characterized by excess reactive oxygen species (ROS) at sites of inflammation.[25] Despite the
29 acknowledged contribution of redox imbalance to asthma,[26,27] ARDS,[28] pulmonary fibrosis,[29] and
30 cancer,[30] as well as the link between these pathologies and MIF, very little structural work has
31 directly addressed the redox behavior of MIF. We wondered whether MIF could utilize redox
32 imbalances to act as a pro-inflammatory sensor to toggle its structure based on the chemical
33 environment of the cell. Altered conformations of MIF at local sites of inflammation could then
34 modulate its function or create different modes of interaction with accessory proteins, thereby
35 controlling downstream biological responses. In a first step toward exploring such a mechanism,
36 we investigated the impact of solution redox conditions on the MIF structure and identified
37 regions of the protein that are sensitive to oxidative environments. We used solution nuclear
38 magnetic resonance (NMR) spectroscopy to assess the redox-dependent dynamics of MIF with
39 spin relaxation experiments and used mass spectrometry to identify redox-modified cysteine
40 residues. We then leveraged these findings, using further NMR structural studies and an *in vivo*
41 assay, to confirm redox-sensitive amino acids as latent points of functional control in MIF.
42
43 **Results**
44 *Oxidizing solution alters MIF structural stability*
45 To assess the effect of solution redox potentials on the MIF structure, we performed far-
46 UV circular dichroism experiments on redox-neutral MIF samples as well as MIF samples that

47 had been oxidized or reduced. CD spectra of redox-altered MIF show characteristic α-β
48 structure, with only minor differences (**Figure S1A**). These data are consistent with numerous
49 MIF structures in the Protein Data Bank (PDB) that have no obvious alterations in the presence
50 of substrates, inhibitors, or mutations. Despite similarly folded structures, temperature-
51 dependent CD experiments (**Figure S1B**) show that an oxidizing environment destabilizes MIF
52 to unfolding relative to reduced and redox-neutral MIF (ΔT_m = - 4.56 °C, $\Delta\Delta G$ = - 2.65 kcal/mol,
53 **Figure S1C**). This energetic difference (expressed per trimer) is modest, but suggests a
54 loosening of the MIF structure that may affect its conformational ensemble.
55
56 *Redox-dependent NMR spectra of MIF highlight multiple conformations and altered dynamics*
57 We used solution NMR to pinpoint regions of the MIF structure that are sensitive to the
58 redox environment. $^{1}H^{15}N$ TROSY-HSQC spectral overlays of reduced, oxidized, and redox-
59 neutral MIF (**Figure S2**) show that while reduced and redox-neutral samples are spectrally
60 similar, more significant spectral changes are observed for MIF under oxidizing conditions.
61 Redox-sensitive chemical shift perturbations (relative to redox-neutral MIF) are observed
62 throughout the protein, including for residues at the N-terminal enzymatic active site, solvent
63 channel, and monomer-monomer interface (**Figures 1A**). Additionally, for oxidized MIF samples,
64 duplicate resonances are observed for 22 residues (**Figures 1B, S3**), suggesting that an
65 oxidizing environment modulates an equilibrium between two conformations of MIF on the NMR
66 timescale. Sites of slow exchange localize to the monomer-monomer interface (**Figure 1C**),
67 indicating that the structure of this region of the protein is strongly affected by oxidizing solution,
68 consistent with the lower thermal stability observed by CD. Perturbations to MIF are not exclusive
69 to redox-active Cys residues, at times occurring 10 - 20 Å from the ^{56}CALC^{59} motif or C80.

However, Cys and Met residues serve as nucleation points for our observations, with a majority of redox-dependent changes to the MIF structure occurring proximal to these traditionally sensitive sites (**Figure S4**). These data are consistent with an alternate oxidized MIF conformation, "oxMIF," most recently probed in a synthetic peptide comprising the MIF ^{56}CALC^{59} sequence.[22]

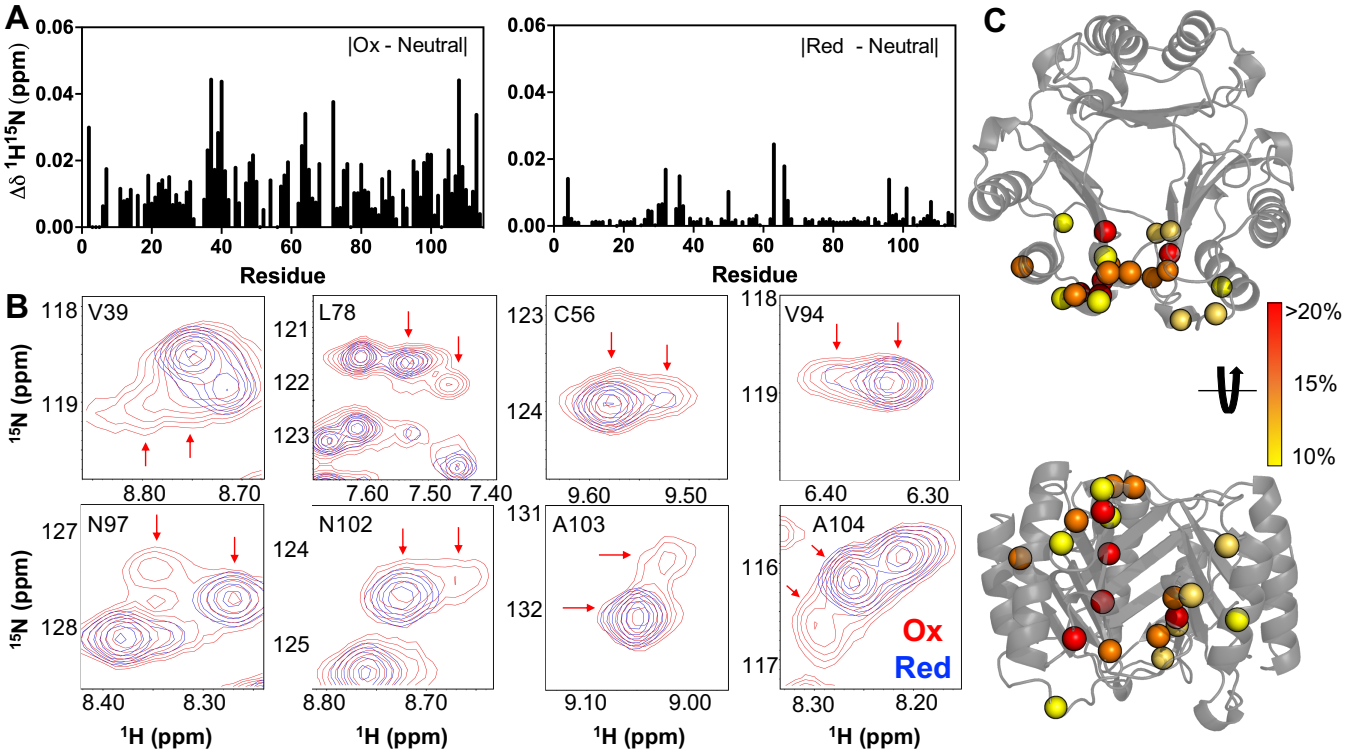

Figure 1. Redox-dependent changes in MIF detected by NMR. **(A)** ^{1}H^{15}N combined chemical shift perturbations ($\Delta\delta$) for oxidized and reduced MIF, relative to a redox-neutral sample. **(B)** Selected resonances from ^{1}H^{15}N HSQC spectral overlays of reduced (blue) and oxidized (red) MIF. Sites of slow exchange observed under oxidizing conditions are indicated by arrows. Populations of MIF conformers determined from the volumes of slow exchange resonances are mapped onto the MIF trimer (PDB: 1MIF) in **(C)**, where the percentage indicated in the legend denotes the minor species (*i.e.* satellite peak). Volumes and populations of slow exchange resonances can be found in Figure S3.

Analysis of longitudinal (R_1) and transverse (R_2) NMR relaxation rates[31] highlights local differences caused by redox conditions. Consistent with the altered thermodynamic parameters of the oxidized MIF samples, individual relaxation rates, as well as the R_1R_2 product, qualitatively

88 imply that MIF exhibits heightened flexibility under oxidizing conditions (**Figure S5A**). Analysis
89 of R_1R_2 values[31] highlights 21 sites suggestive of μs – ms flexibility in oxMIF (R_1R_2 >1.5σ above
90 the 10% trimmed mean of the data), 7 of which do not appear flexible in both redox-neutral and
91 reduced MIF. Despite local patches of altered flexibility, the dynamic profiles of reduced and
92 redox-neutral MIF are similar to each other. ^{1}H-[^{15}N] NOE values and order parameters also hint
93 at patches of local flexibility in oxMIF, though fast timescale dynamics do not differ substantially
94 between samples. Residues with relaxation parameters suggestive of μs – ms flexibility are
95 mapped onto the MIF trimer and monomer structures in **Figure S5**. Correlation plots of R_1R_2
96 and S^2 parameters for reduced and oxidized MIF reveal a weaker correlation for R_1R_2,
97 suggesting that MIF experiences greater dynamic changes on the μs – ms timescale over a
98 range of redox conditions (**Figure 2A**). Contributions to the variations in R_1R_2 parameters are
99 most strongly affected by oxidizing solution conditions (**Figure 2B, left panel**), while reducing
100 conditions contribute more significantly to the ps – ns dynamics of MIF via S^2 (**Figure 2B, right**
101 **panel**). Redox-sensitive residues with apparent μs – ms flexibility include T30, G50, L58, S63,
102 I64*, K66, R73, L83, A84, R86, R93, I96, N97*, N109*, N110, T112, and A114, and those with
103 apparent ps – ns fluctuations are F3, T7, L26, T30, D44, I64*, K66, K77, L83, L87, S90, Y95*,
104 D100, A103, and S111* (**Figure 3C**). Asterisks indicate residues previously identified as
105 controlling MIF enzymatic activity and CD74 activation via direct interaction or through allosteric
106 signaling,[6,32,33] indicating redox-dependent perturbations in MIF may have functional
107 consequences.

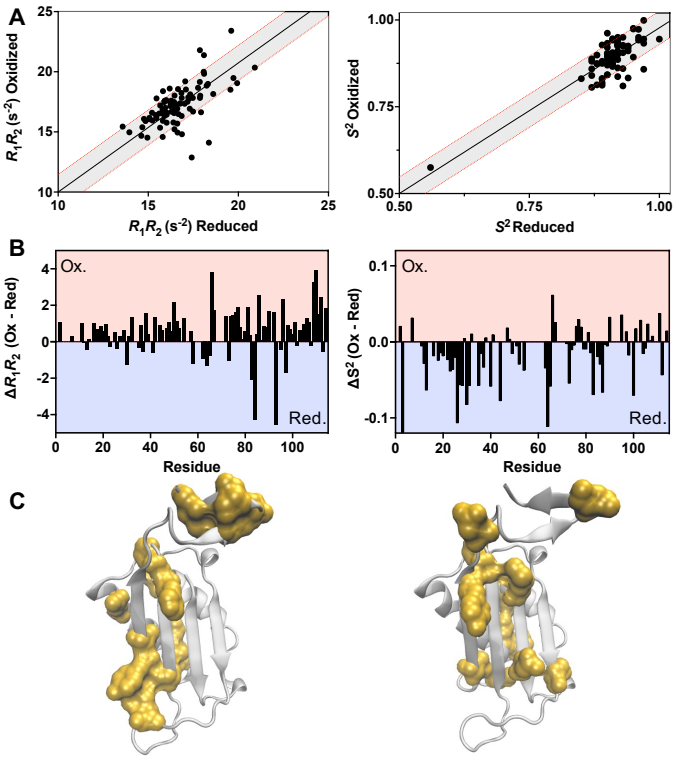

Figure 2. (A) Correlation plots of the R_1R_2 (left) and S^2 (right) parameters for oxidized and reduced MIF. Gray shaded areas represent ±1.5σ from the linear least-squares fits of the data (black lines). **(B)** Per-residue differences in R_1R_2 (left) and S^2 (right) plotted as oxidized – reduced. Bars in the shaded red area denote a greater value in oxMIF, while those in the blue area denote a greater value in reduced MIF. **(C)** Residues outside of the 1.5σ correlation boundaries in **(A)** are mapped onto the MIF monomer (PDB: 1MIF), highlighting regions of the protein with redox-dependent differences in μs – ms (left) and ps – ns (right) dynamics.

To confirm the influence of solution redox potential on μs – ms dynamics in MIF, we quantified the exchange contribution to transverse relaxation, R_{ex}, via CPMG relaxation dispersion experiments. The average global R_{ex} value (<R_{ex}>) for MIF is fairly similar across the redox regimes tested, with local differences arising primarily under oxidizing conditions (**Figure 3A**). Numerous sites of μs – ms dynamics are observed in all redox-modulated MIF samples (**Figure S6**), however, oxidizing solution stimulates the most widespread relaxation dispersion, affecting 39 residues (~34 %) in the MIF structure. These data are consistent with R_1R_2 values that estimated a stronger contribution from oxidizing solution to μs – ms motions (**Figure 2**).

125 Regions of MIF with known functional importance become flexible, including the monomer
126 interface (L26, I37, G50) and solvent channel allosteric site (I96, Y99). Despite similar dynamics
127 in large portions of MIF, **Figure 3B** highlights selected sites that only appear flexible under
128 oxidizing conditions. With the exception of the solvent channel, these flexible sites have not been
129 well characterized for functional impact, suggesting that studies of MIF redox dependence can
130 reveal new target residues for structure-function correlations.

131

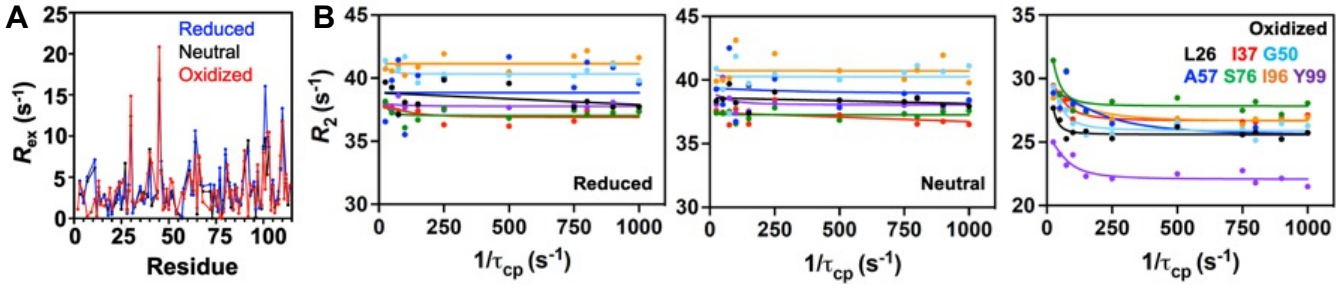

132

133 **Figure 3. (A)** Per-residue exchange contribution to relaxation (R_{ex}) for reduced (blue), redox-
134 neutral (black), and oxidized MIF (red). **(B)** CPMG relaxation dispersion profiles for selected MIF
135 residues collected in reducing (left), redox-neutral (center), or oxidizing (right) solution. These
136 sites display evidence of μs – ms flexibility under oxidizing conditions.
137

138 *Cysteine 80 is a selectively modified redox switch*

139 Prior work with a MIF epitope[22] suggested that C80 functions as a redox molecular switch.
140 However, redox sensitivity of C80 in the full-length trimeric protein is unknown. We performed
141 quantitative mass spectrometry to explore the possibility that C80 could be selectively modified
142 by redox reagents. Stepwise alkylation of MIF under each redox condition with iodoacetamide
143 (IAA) and N-ethylmaleimide (NEM) yields critical insight into the oxidation state of C80 in the
144 intact MIF trimer (**Figures 4, S7, S8**). Using NEM-bound C80 as a proxy for the abundance of
145 cystine residues reveals an increase from 75.1% to 91.3% cystine abundance between redox-
146 neutral and oxidizing conditions (**Figure 4B**). Under redox-neutral conditions, C80 exhibits the

147 greatest variance in cystine abundance, further highlighting the reactivity and sensitivity of this
148 residue to environmental conditions. The relative abundance of cystine is also sensitive to the
149 amount of oxidative stress (**Figure S8A**). Increasing the concentration of oxidant in solution from
150 1:1 to 2:1 shifts the C80 cystine relative abundance from 83.1% to 91.3%. For comparison,
151 **Figure S7B** shows the expected contributions to the total ion intensity of C80 modified with IAA
152 or NEM if C80 is in a fully reduced, 50% reduced, or fully oxidized state. In addition to C80, MIF
153 also contains two cysteine residues in its ^{56}CALC^{59} motif; however, the peptide fragment
154 containing C56 and C59 is a large 34-mer, precluding quantitation by the MS methods utilized
155 here. Although we focus on C80, we cannot rule out a significant role for other cysteines in MIF
156 redox dependence.

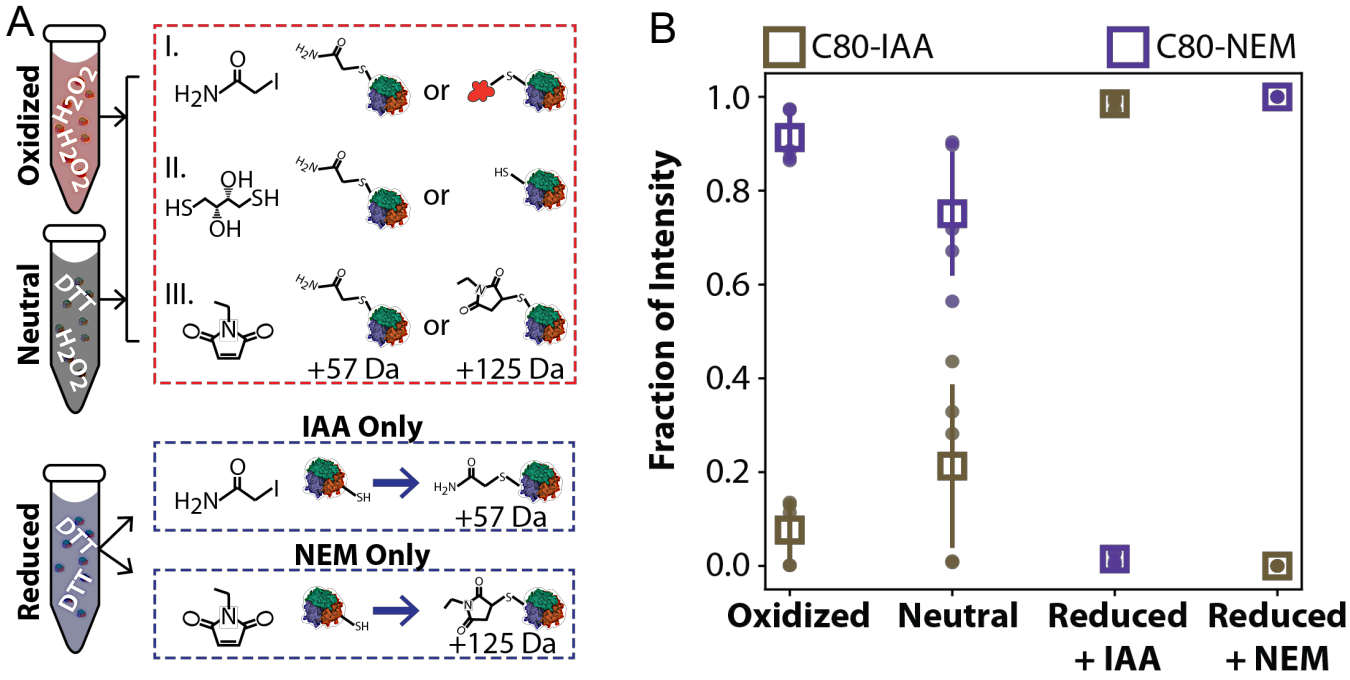

157

158 **Figure 4. (A)** Stepwise alkylation of MIF cysteine residues to determine the relative abundance
159 of oxidized residues via mass spectrometry. The alkylation workflow involved three reaction
160 steps (red, top panel). MIF equilibrated under reducing conditions was treated with only one
161 alkylating agent and served as a quantitative control (blue, bottom panels). **(B)** Relative
162 quantitation of C80 alkylation revealed conformational dependence and sensitivity to the
163 surrounding redox environment.
164

165 *Mutation of redox-sensitive residues alters MIF structure and biological function*

166 To test the possibility that the redox sensitivity of MIF could reveal sites of functional
167 impact that are not otherwise obvious, we created single point mutations at two residues
168 displaying redox-dependent structural and/or dynamic changes, lysine 66 (K66) and cysteine 80
169 (C80). K66 was found to have a large variation in the R_1R_2 parameter in oxMIF, as well as a low
170 ^{1}H-[^{15}N] NOE in reduced MIF (Figures 2, S5), indicating that it undergoes significant changes in
171 flexibility between the oxidized and reduced states. C80 also exhibits dynamic changes
172 suggestive of redox-altered μs – ms chemical exchange and was shown by mass spectrometry
173 to be selectively modified under oxidizing conditions (Figures 4, S5-8). ^{1}H^{15}N TROSY-HSQC
174 NMR spectra of the K66A and C80A variants were collected in redox-neutral, reducing, and
175 oxidizing solutions. Baseline structural changes caused by the K66A and C80A mutations are
176 significant under redox-neutral conditions, particularly for the C80A variant, though CD
177 spectroscopy indicates the variants are fully folded at NMR sample temperatures (Figures S9,
178 S10). Interestingly, chemical shift perturbations observed for K66A MIF under oxidizing and
179 reducing conditions are modest when compared to a redox-neutral K66A sample (Figures 5A,
180 5B). Most notably, oxidized K66A exhibits a chemical shift profile much smaller in magnitude
181 than that observed in the corresponding wt-MIF experiments. In addition, reduced K66A exhibits
182 larger chemical shift perturbations than oxidized in both number and magnitude, the inverse of
183 what was found for wt-MIF. These data alone suggest that K66 may play a role in modulating
184 the redox-dependent structural changes of wt-MIF, which are substantially diminished upon
185 mutation. Likewise, the C80A variant strongly attenuates redox-sensitive NMR chemical shift
186 changes in both reduced and oxMIF. These data, along with mass spectrometry, indicate that
187 C80 modulates the conformational landscape of MIF under oxidative conditions.

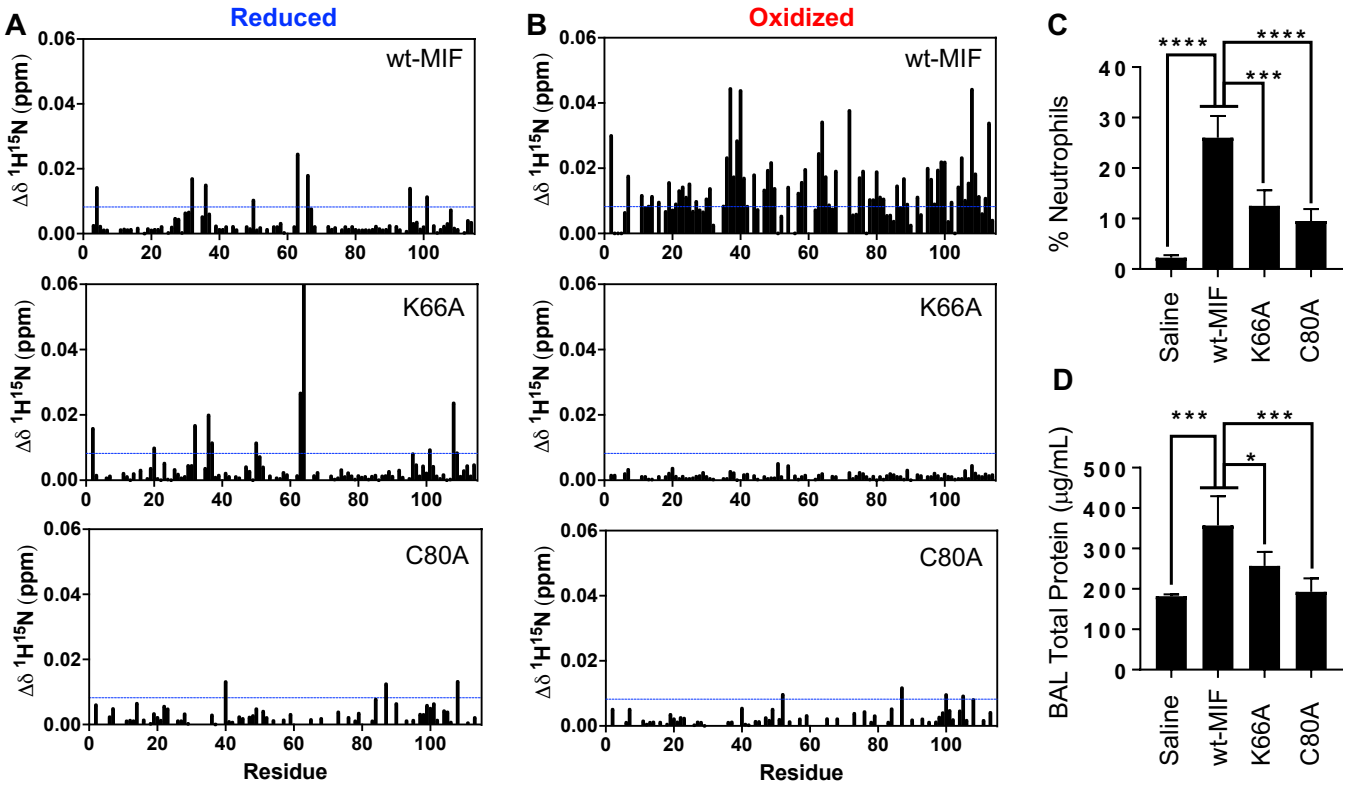

Figure 5. Mutation of the redox-sensitive K66 and C80 residues alters the redox-dependent MIF structure and hinders the ability of MIF to activate CD74 *in vivo*. K66A and C80A mutations alter the combined ^{1}H-^{15}N chemical shift profiles of reduced **(A)** and oxidized **(B)** MIF, relative to redox-neutral K66A and C80A samples used as references. Blue lines denote 1.5σ above the 10% trimmed mean of all shifts. Combined ^{1}H-^{15}N chemical shift plots for reduced and oxidized wt-MIF are repeated here from Figure 1 for comparison. **(C)** K66A and C80A mutations significantly decreased CD74-dependent neutrophil recruitment in murine lungs *in vivo*. **(D)** Attenuated CD74-dependent neutrophil recruitment by K66A and C80A also led to significantly decreased pulmonary edema *in vivo*. (n = 4 in each group, *p<0.05, ***p≤0.001 and ****p≤0.0001). Data are expressed as mean ± SEM.

To understand whether this altered redox behavior foreshadowed changes in MIF function, we evaluated the K66A and C80A variants in neutrophil recruitment assays in murine lungs, where we measured total immune cells, percentage of neutrophils in BAL fluid, and protein content (as a marker of alveolar capillary leak/pulmonary edema). This *in vivo* assay quantifies neutrophil recruitment on the surface of alveolar macrophages, an established metric for the

205 MIF-induced activation of the pro-inflammatory CD74 receptor.[34] The assay is indirect, using
206 chemokines released by activated macrophages to stimulate CXCR2 receptors on neutrophils
207 (that do not directly express CD74) to induce their migration to murine lungs.[35] We found that
208 wt-MIF significantly increased the total BAL fluid cell counts over saline controls, while the K66A
209 and C80A variants showed a reduced number of total BAL fluid immune cells (**Figure S11**). The
210 neutrophil influx and pulmonary edema protein levels were significantly increased in the wt-MIF
211 group relative to vehicle controls (**Figures 5C, 5D**). In contrast, we observed significant
212 decreases in the groups to which the MIF variants were delivered, as compared to wt-MIF.
213 Together, our data indicate that the K66A and C80A variants have a functional effect in reducing
214 the inflammatory response of MIF in the murine lung. These findings also suggest that structural
215 and/or dynamic sensitivity of residues within MIF can provide a novel route for achieving
216 functional control beyond the known MIF active sites.

217 **Discussion**

218 We used solution redox potentials to modulate the MIF structure and dynamics in order
219 to reveal changes in conformational equilibria and redox-sensitive residues that may be latent
220 functional sites within its structure. This work builds upon prior studies implying redox sensitivity
221 of MIF[11,22,36,37] as well as our recent paper highlighting a series of allosteric residues linking the
222 enzymatic (tautomerase) and CD74 binding sites of MIF.[38] Here, we demonstrate that
223 examination of MIF redox sensitivity is another useful avenue for probing function beyond its
224 established active sites. Since MIF participates in both intracellular and extracellular
225 interactions,[39] where the redox environments differ, understanding the implications of its redox
226 dependence may also inform its pro-inflammatory mechanisms and functional promiscuity,
227 which has been investigated at the biochemical, but not the structural, level. A previous

228 characterization of the association of MIF with p53 tumor suppressor suggested the interaction
229 to be redox-dependent, having shown a significant decrease in coprecipitation in the presence
230 of a reductant.[40] Further, interaction of MIF with ribosomal protein S-19 (RPS-19) was shown to
231 occur more strongly under reducing conditions.[41] In addition, MIF is known to be post-
232 translationally modified by glycation in the brain tissue of Alzheimer's patients. Most notably, an
233 altered electrophoretic migratory behavior of glycated MIF was observed and demonstrated *in*
234 *vitro* by incubating MIF with glucose under oxidizing conditions.[42]

235 Redox signatures of inflammatory diseases, most of which implicate MIF, can also be
236 markedly different from those of healthy humans. The redox potential of epithelial lining fluid is -
237 110 to -40 mV in the lungs of asthmatics, which is significantly more oxidizing than that of healthy
238 humans (-150 to -200 mV).[27] Further, the synovial fluid of rheumatoid arthritis patients has been
239 shown to be highly oxidizing relative to that of a non-arthritic control group.[43,44] A significant body
240 of literature suggests that when overexpressed at sites of inflammation,[16] MIF can endure large
241 swings in environmental redox potential, consistent with our determination of the MIF redox
242 potential *in vitro* using solution NMR[45,46] (**Figure S12**, midpoint E_0' = -215 $\pm$ 5 mV, near normal
243 physiological range). NMR spin relaxation studies show redox-dependent modulation of local
244 flexibility in MIF, with motion observed on multiple timescales. oxMIF, in particular, exhibits the
245 most significant structural and dynamic changes, with widespread NMR spectral perturbations
246 and CPMG relaxation dispersion that show oxidizing potentials stimulate flexibility in ~34% of
247 the MIF structure, including its redox-active residues. However, the majority of these flexible
248 regions have not been confirmed to harbor any functional impact in prior work.

249 It remains unclear how this relatively compact (12.5 kDa monomer) and symmetrical
250 homotrimer accommodates a wide range of non-overlapping activities. A 2018 study showed

251 that nanosecond dynamics were important for organization of the MIF-CD74 binding interface,[6]
252 and studies of a MIF epitope containing its ^{56}CALC^{59} motif showed selective binding to the Fab
253 fragment of the BaxB01 antibody under oxidizing conditions, after rearrangement of the Cys
254 sulfhydryls.[22] Oxidizing conditions appear to promote a more flexible solvent channel, which we
255 recently showed to be central to an allosteric mechanism regulating tautomerase and CD74
256 activation involving motion on multiple timescales.[38] Given the number of MIF functions that have
257 yet to be explored at the molecular level and the fact that ~100 X-ray crystal structures of MIF
258 mutants, substrate-, and inhibitor-bound complexes have negligible variation in static structure
259 but vastly different NMR spectra, it is plausible, if not likely, that additional regions of functional
260 importance exist in MIF.

261 Here, we asked if changes in solution redox potential could reveal some of these latent
262 sites by modulating the structural and/or dynamic signatures of MIF. We experimentally altered
263 the redox potential of wt-MIF NMR samples, enabling us to identify redox-dependent structural
264 changes in residues that may be important for function. We mutated two such residues, K66 and
265 C80, that showed redox-sensitivity in wt-MIF and observed structural effects on MIF redox
266 behavior as well as altered functional responses. Having further confirmed the propensity of C80
267 for redox-driven modification by mass spectrometry, we speculate that MIF could act as a sensor
268 that toggles its conformation depending on its cellular environment to engage with varied binding
269 partners, as was previously suggested in a conformational control scheme for the ^{56}CALC^{59}
270 motif. The more extensive but partially-overlapping set of residues affected by the redox
271 environment suggests the regulatory network controlling non-overlapping MIF functions may be
272 larger than previously reported, where additional “allosteric nodes” may be revealed only when
273 MIF is exposed to stimuli, such as environmental factors associated with inflammation, serving

274 as a natural means of activating latent residues to expand MIF functions under altered cellular
275 conditions. Speculating further, targeting small molecules to redox sensitive residues may
276 prevent MIF from engaging in certain downstream cascades. Future studies of protein-protein
277 interactions with supposed binding partners of MIF, such as thioredoxin[47,48] or ribosomal protein
278 S19,[41] as well as with small molecules, can evaluate this mechanism. Another interesting avenue
279 warranting further exploration is the redox-dependent interaction of MIF with its known inhibitors
280 or with novel compounds, as it presents an opportunity to preferentially target oxMIF, a form of
281 the protein that may appear predominately within the inflammatory state.
282

283 **Materials and Methods**

284 *Protein expression, purification, and redox sample preparation*

285 Wild-type (wt) and/or human MIF variants cloned into a pET11b vector were grown in
286 lysogeny broth (LB) for biochemical studies and in isotopically enriched M9 minimal medium
287 supplemented with $CaCl_2$, $MgSO_4$, and MEM vitamins for NMR, after adapting BL21(DE3) cells
288 to D_2O. Small cultures of MIF were grown overnight in LB at 37 °C and used to inoculate cultures
289 containing 50% D_2O the following morning, which were grown 8 – 10 hours at 37 °C and then
290 used to inoculate cultures containing 95% D_2O, which were incubated at 37 °C for 12 hours. The
291 cells were collected by centrifugation and resuspended in M9 medium (1 L, 100% D_2O)
292 supplemented with $^{15}NH_4Cl$ (Cambridge Isotope Laboratories) and $^{12}C_6H_{12}O_6$ as the sole
293 nitrogen and carbon sources, respectively. Cultures were grown to an OD_{600} of 0.8 – 1.0 and
294 induced with 1 mM isopropyl β-D-1-thiogalactopyranoside (IPTG). Following 16-18 hours of post-
295 induction growth, the cells were harvested by centrifugation.

296 The cells were resuspended in ~30 mL of an ice-cold buffer of 20 mM Tris-HCl, 20 mM
297 NaCl, and 1 mM EDTA at pH 7.4 supplemented with protease inhibitors, lysed by ultrasonication,
298 clarified by centrifugation, filtered, and purified with a 120 mL Macro-Prep High Q
299 column(BioRad) pre-equilibrated with the lysis buffer. MIF does not bind the Q resin and is found
300 in the flow-through. MIF was purified to its final form on a HiLoad 26/600 Superdex 200 size
301 exclusion column (GE Healthcare). For NMR samples, MIF was dialyzed into a buffer containing
302 20 mM sodium phosphate, 1 mM EDTA, and 7.5% D_2O at pH 7.0. Final concentrations of MIF
303 were 0.5 – 1 mM determined using ε_{280} = 12,950 M^{-1} cm^{-1}.[49]

304 Oxidation of MIF was achieved by addition of H_2O_2 to a final concentration of 6 mM in an
305 aliquot of 0.5 – 1 mM MIF. Reduced MIF was prepared with a 6 mM final concentration of DTT.
306 Redox-neutral samples were prepared with equimolar amounts of DTT/H_2O_2. Stocks of the
307 oxidizing and reducing agents were freshly prepared in a degassed buffer of 20 mM sodium
308 phosphate, 1 mM EDTA, and 7.5% D_2O at pH 7.0. Following addition of oxidant or reductant to
309 MIF samples, the NMR tubes were briefly degassed with nitrogen and sealed with Parafilm
310 (Bemis). The samples were equilibrated in the presence of redox reagents for at least six hours.

311 *Circular Dichroism (CD) Spectroscopy*

312 CD spectra and thermal unfolding experiments were recorded on a JASCO J-815
313 spectropolarimeter equipped with a variable temperature Peltier device. Denaturation curves of
314 10 μM MIF were recorded at 218 nm in a 2 mm quartz cuvette. The temperature range for each
315 scan was 20 – 100 °C (293 K – 373 K). Thermodynamic parameters were extracted via nonlinear
316 curve fitting of CD data to **Equation 1** in GraphPad Prism:

317 $$Ellipticity\ (T) = \frac{[(m_f T + b_f) + (m_u T + b_u)]exp\left[\left(-\frac{\Delta H_{D,vH}}{R}\right)\left(\frac{1}{T} - \frac{1}{T_m}\right)\right]}{1 + exp\left[\left(-\frac{\Delta H_{D,vH}}{R}\right)\left(\frac{1}{T} - \frac{1}{T_m}\right)\right]} \quad (1)$$

where m_f, b_f, and m_u, b_u are the slopes and y-intercepts of the folded (low temperature) and unfolded (high temperature) regions of the melting curve, R is the gas constant, T_m and $\Delta H_{D,vH}$ are the unfolding midpoint and van't Hoff enthalpy of denaturation at T_m, respectively. Free energy analysis was performed as described elsewhere,[50] using values of ΔC_p, the unfolding heat capacity, estimated from the report of Privalov.[51,52] The differences in apparent unfolding enthalpies, entropies, and free energies at a reference temperature (T_{REF}) of 298 K were calculated as;

$$\Delta H_{D,app} = \Delta H_{D,vH} + \Delta C_p(T_{REF} - T_m) \quad (2)$$

$$\Delta S_{D,app} = \frac{\Delta H_{D,vH}}{T_m} + \Delta C_p ln\left(\frac{T_{REF}}{T_m}\right) \quad (3)$$

$$\Delta G(T) = \Delta H_{D,vH}\left(1 - \frac{T_{REF}}{T_m}\right) + \Delta C_p\left[(T_{REF} - T_m) - T_{REF} ln\left(\frac{T_{REF}}{T_m}\right)\right] \quad (4)$$

These data are reported as "apparent" values due to the ~90% reversibility of the MIF unfolding transition.

NMR Spectroscopy

NMR experiments were performed on a Bruker Avance NEO 600 MHz or Bruker Avance III HD 850 MHz spectrometer at 30 °C. NMR data were processed using NMRPipe[53] and analyzed in Sparky[54] along with in-house scripts. The pH of NMR samples was monitored after addition of redox reagents to ensure that NMR spectral changes were due to reduction/oxidation. NMR assignments for wt-MIF and the K66A and C80A variants were confirmed from standard triple resonance experiments. Combined chemical shift perturbations ($\Delta\delta$) were determined by $\Delta\delta = \sqrt{(\delta_{HN}^2) + (\delta_N^2/25)}$. The HSQC of oxidized MIF was processed with an exponential window function in both the direct and indirect dimensions in NMRPipe. The peak intensity and volume for each pair of slow exchanging peaks were

340 calculated in SPARKY, where peak volume was calculated by integrating each peak as a
341 Lorentzian. The minor state populations were estimated by taking the volume of the minor
342 peak and dividing by the total volume of the slow exchanging pairs.

343 NMR spin relaxation experiments were performed using TROSY-based pulse
344 sequences adapted from Palmer and coworkers.[55] Relaxation data were acquired with the ^{1}H
345 and ^{15}N carriers set to the water resonance and 120 ppm, respectively. Longitudinal relaxation
346 rates (R_1) were measured with T_1 delays of 0, 20, 60, 100, 200, 600, 800, and 1200 ms.
347 Transverse relaxation rates (R_2) were collected with 1.0 ms spacing between 180° CPMG
348 pulses at total relaxation delays of 0, 1, 2, 4, 8, and 10, and 12 ms. The recycle delay in these
349 experiments was 2.5 s. Longitudinal and transverse relaxation rates were extracted by non-
350 linear least squares fitting of the peak heights (major peaks in cases of slow exchange) to a
351 single exponential decay using in-house software. Uncertainties in these rates were
352 determined from replicate spectra. The heteronuclear cross-relaxation rate (^{1}H-[^{15}N] NOE) was
353 obtained by interleaving pulse sequences with and without proton saturation and calculated
354 from the ratio of peak heights from these experiments. Carr-Purcell-Meiboom-Gill (CPMG)
355 NMR experiments were performed at 30 ºC with a constant relaxation period of 40 ms, a 2.0 s
356 recycle delay, and τ_{cp} points of 0, 25, 50, 75, 100, 150, 250, 500, 750, 800, 900, and 1000 ms.
357 Relaxation dispersion profiles were generated by plotting R_2 vs. $1/\tau_{cp}$ and exchange
358 parameters were obtained from fits of these data carried out with in-house scripts.
359 Uncertainties were obtained from replicate spectra.

360 NMR spin-relaxation rates were fit to one of five semi-empirical forms of the spectral
361 density function using model-free analysis.[56,57] Fitting of motional parameters was performed in
362 RELAX.[58,59] The criteria for inclusion of residues in the diffusion tensor estimate relied on the

363 method of Tjandra and coworkers.[47] N-H bond lengths were assumed to be 1.02 Å and the ^{15}N
364 chemical shift anisotropy was set to -160 ppm. During the model selection process, the diffusion
365 tensor parameters were optimized simultaneously, and model selection was repeated until the
366 optimized tensor parameters and order parameter (S^2) did not differ from those of the previous
367 iteration.

368 *Mass Spectrometry*

369 Cysteine and cystine residues of purified MIF equilibrated under each of the redox
370 conditions were alkylated in a stepwise process with iodoacetamide (IAA) followed by *N*-
371 ethylmaleimide (NEM). Parallel reaction monitoring-mass spectrometry captured the oxidation
372 states of C80 under different redox conditions. Skyline software[60] was used to calculate the
373 relative abundance of cysteine and cystine at the C80 position, indicated by binding to IAA or
374 NEM. Additional methodological details can be found in the **Supporting Information**.

375 *In Vivo Neutrophil Recruitment Assay*

376 All animal studies were approved by the Institutional Animal Care and Use Committee of
377 Cooper University Healthcare, Camden, NJ. The wt mice of genetic background strain
378 (C57BL6/J) were purchased from the Jackson Laboratory (Bar Harbor, ME). Mice were housed
379 at the pathogen-free animal facility at Cooper University Healthcare. All experiments were done
380 in 9-10 week old male mice. Mice were administered a one-time intratracheal instillation of 100
381 µl of normal saline alone (vehicle) or normal saline solution containing 1 µg of wt-MIF, K66A MIF
382 or C80A MIF. These mice were sacrificed after 6 h of vehicle only or vehicle + experimental
383 agent administration. Bronchoalveolar lavage (BAL) was performed by cannulating the trachea
384 with a blunt 22-gauge needle and lavaging both lungs with 800 µl of sterile PBS solution.
385 Bronchoalveolar lavage fluid (BALF) was harvested, and total cell counts in BALF were

386 determined using the TC20 automated cell counter (Bio-Rad Laboratories, Inc., Hercules, CA).
387 The differential cell counts were performed on cells cytocentrifuged onto glass slides (Fisher
388 Scientific) stained with the Hema 3 Staining System (Fisher Diagnostics, Middletown, VA) and
389 cell differential was tabulated using light microscopy. Total protein concentration in the BAL fluid
390 was measured using the Pierce™ BCA assay kit (Thermo Scientific, Rockford, IL), as previously
391 described.[6]
392

393 **Acknowledgments**

394 The authors thank J. Patrick Loria for helpful discussions. This work was supported by Rhode
395 Island Foundation Grant GR5290658 and funds from the Office of the Vice President for
396 Research at Brown University (to GPL).
397

398 **Competing Interests**

399 The authors declare no competing interests.
400

401 **References**

402 (1) Bernhagen, J. r.; Bucala, R.: MIF Family Cytokines in Innate Immunity and Homeostasis.
403 In *Progress in Inflammation Research,*; 1st ed.; Springer International Publishing : Imprint: Springer,:
404 Cham, 2017.
405 (2) Leng, L.; Metz, C. N.; Fang, Y.; Xu, J.; Donnelly, S.; Baugh, J.; Delohery, T.; Chen, Y.;
406 Mitchell, R. A.; Bucala, R. MIF signal transduction initiated by binding to CD74. *J Exp Med* **2003**, *197*,
407 1467-1476.
408 (3) Bernhagen, J.; Krohn, R.; Lue, H.; Gregory, J. L.; Zernecke, A.; Koenen, R. R.; Dewor,
409 M.; Georgiev, I.; Schober, A.; Leng, L.; Kooistra, T.; Fingerle-Rowson, G.; Ghezzi, P.; Kleemann, R.;
410 McColl, S. R.; Bucala, R.; Hickey, M. J.; Weber, C. MIF is a noncognate ligand of CXC chemokine
411 receptors in inflammatory and atherogenic cell recruitment. *Nat Med* **2007**, *13*, 587-596.
412 (4) Meyer-Siegler, K. L.; Iczkowski, K. A.; Leng, L.; Bucala, R.; Vera, P. L. Inhibiton of
413 Macrophage Migration Inhibitory Factor or its Receptor (CD74) Attenuates Growth and Invasion of DU-
414 145 Prostate Cancer Cells. *J. Immunol.* **2006**, *177*, 8730-8739.

415 (5) Cournia, Z.; Leng, L.; Gandavadi, S.; Du, X.; Bucala, R.; Jorgensen, W. L. Discovery of
416 Human Macrophage Migration Inhibitory Factor (MIF)-CD74 Amtagonists via Virtual Screening. *J. Med.*
417 *Chem.* **2009**, *52*, 416-424.
418 (6) Pantouris, G.; Ho, J.; Shah, D.; Syed, M. A.; Leng, L.; Bhandari, V.; Bucala, R.; Batista,
419 V. S.; Loria, J. P.; Lolis, E. J. Nanosecond Dynamics Regulate the MIF-induced Activity of CD74. *Angew.*
420 *Chem. Int. Ed.* **2018**, *57*, 7116-7119.
421 (7) Mizue, Y.; Ghani, S.; Leng, L.; McDonald, C.; Kong, P.; Baugh, J.; Lane, S. J.; Craft, J.;
422 Nishihira, J.; Donnelly, S. C.; Zhu, Z.; Bucala, R. Role for Macrophage Migration Inhibitory Factor in
423 Asthma. *Proc. Natl. Acad. Sci. USA* **2005**, *102*, 14410-14415.
424 (8) Joshi, P. C.; Poole, G. V.; Sachdev, V.; Zhou, X.; Jones, Q. Trauma Patients with Positive
425 Cultures have Higher Levels of Circulating Macrophage Migration Inhibitory Factor. *Res. Commun. Mol.*
426 *Pathol. Pharmacol.* **2000**, *107*, 13-20.
427 (9) Kleeman, R.; Hausser, A.; Geiger, G.; Mischke, R.; Burger-Kentischer, A.; Flieger, O.;
428 Johannes, F. J.; Roger, T.; Calandra, T.; Kapurniotu, A.; Grell, M.; Finkelmeier, D.; Brunner, H.;
429 Bernhagen, J. Intracellular Action of the Cytokine MIF to Modulate AP-1 Activity and the Cell Cycle
430 Through JAB-1. *Nature* **2000**, *408*, 211-216.
431 (10) Calandra, T.; Bernhagen, J.; Metz, C. N.; Spiegel, L. A.; Bacher, M.; Donnelly, T.; Cerami,
432 A.; Bucala, R. MIF as a Glucocorticoid-Induced Modulator of Cytokine Production. *Nature* **1995**, *377*,
433 68-71.
434 (11) Thiele, M.; Bernhagen, J. Link between Macrophage Migration Inhibitory Factor and
435 Cellular Redox Regulation. *Antioxid. Redox Signal.* **2005**, *7*, 1234-1248.
436 (12) Morand, E. F.; Leech, M.; Bernhagen, J. MIF: A New Cytokine Link between Rheumatoid
437 Arthritis and Atherosclerosis. *Nat. Rev. Drug Discov.* **2006**, *5*, 399-410.
438 (13) de Jong, Y. P.; Abadia-Molina, A. C.; Satoskar, A. R.; Clarke, K.; Rietdijk, S. T.; Faubion,
439 W. A.; Mizoguchi, E.; Metz, C. N.; Alsahli, M.; ten Hove, T.; Keates, A. C.; Lubetsky, J. B.; Farrell, R.
440 J.; Michetti, P.; van Deventer, S. J.; Lolis, E.; David, J. R.; Bhan, A. K.; Terhorst, C. Development of
441 Chronic Colitis is Dependent on the Cytokine MIF. *Nat. Immunol.* **2001**, *2*, 1061-1066.
442 (14) Makhija, R.; Kingsnorth, A.; Demaine, A. Gene Polymorphisms of the Macrophage
443 Migration Inhibitory Factor and Acute Pancreatitis. *J.Pancreas* **2007**, *8*, 289-295.
444 (15) Donnelly, S. C.; Haslett, C.; Reid, P. T.; Grant, I. S.; Wallace, W. A.; Metz, C. N.; Bruce,
445 L. J.; Bucala, R. Regulatory Role for Macrophage Migration Inhibitory Factor in Acute Respiratory
446 Distress Syndrome. *Nat. Med.* **1997**, *3*, 320-323.
447 (16) Bucala, R.; Donnelly, S. C. Macrophage Migration Inhibitory Factor: A Probable Link
448 between Inflammation and Cancer. *Immunity* **2007**, *26*, 281-285.
449 (17) Balogh, K. N.; Templeton, D. J.; Cross, J. V. Macrophage Migration Inhibitory Factor
450 Protects Cancer Cells from Immunogenic Cell Death and Impairs Anti-tumor Responses. *PLOS One* **2018**,
451 *13*, e0197702.
452 (18) Richard, V.; Kindt, N.; Saussez, S. Macrophage Migration Inhibitory Factor Involvement
453 in Breast Cancer. *Int. J. Oncol.* **2015**, *47*, 1627-1633.
454 (19) Agarwal, R.; Whang, D. H.; Alvero, A. B.; Visintin, I.; Lai, Y. L.; Segal, E. A.; Schwartz,
455 P.; Ward, D.; Rutherford, T.; Mor, G. Macrophage Migration Inhibitory Factor Expression in Ovarian
456 Cancer. *Am. J. Obstet. Gynecol.* **2007**, *196*, 348.e341-348.e345.
457 (20) Nobre, C. C. G.; de Arajuo, J. M. G.; Fernandes, T. A. A. M.; Cobucci, R. N. O.; Lanza,
458 D. C. F.; Andrade, V. S.; Fernandes, J. V. Macrophage Migration Inhibitory Factor (MIF): Biological
459 Activities and Relation with Cancer. *Pathol. Oncol. Res.* **2017**, *23*, 235-244.

460 (21) Bleilevens, C.; Soppert, J.; Hoffmann, A.; Breuer, T.; Bernhagen, J.; Martin, L.; Stiehler,
461 L.; Marx, G.; Dreher, M.; Stoppe, C.; Simon, T. P. Macrophage Migration Inhibitory Factor (MIF) Plasma
462 Concentration in Critically Ill COVID-19 Patients: A Prospective Observational Study. *Diagnostics*
463 *(Basel)* **2021**, *11*.
464 (22) Schinagl, A.; Kerschbaumer, R. J.; Sabarth, N.; Douillard, P.; Scholz, P.; Voelkel, D.;
465 Hollerweger, J. C.; Goettig, P.; Brandstetter, H.; Scheiflinger, F.; Thiele, M. Role of the Cysteine 81
466 Residue of Macrophage Migration Inhibitory Factor as a Molecular Redox Switch. *Biochemistry* **2018**,
467 *57*, 1523-1532.
468 (23) Kleemann, R.; Kapurniotu, A.; Frank, R. W.; Gessner, A.; Mischke, R.; Flieger, O.; Juttner,
469 S.; Brunner, H.; Bernhagen, J. Disulfide analysis reveals a role for macrophage migration inhibitory factor
470 (MIF) as thiol-protein oxidoreductase. *J Mol Biol* **1998**, *280*, 85-102.
471 (24) Kleemann, R.; Mischke, R.; Kapurniotu, A.; Brunner, H.; Bernhagen, J. Specific reduction
472 of insulin disulfides by macrophage migration inhibitory factor (MIF) with glutathione and
473 dihydrolipoamide: potential role in cellular redox processes. *FEBS Lett* **1998**, *430*, 191-196.
474 (25) Mittal, M.; Siddiqui, M. R.; Tran, K.; Reddy, S. P.; Malik, A. B. Reactive oxygen species
475 in inflammation and tissue injury. *Antioxid Redox Signal* **2014**, *20*, 1126-1167.
476 (26) Fahy, J. V.; Corry, D. B.; Boushey, H. A. Airway Inflammation and Remodeling in
477 Asthma. *Curr. Opin. Pulm. Med.* **2000**, *6*, 15-20.
478 (27) Fitzpatrick, A. M.; Teague, W. G.; Holguin, F.; Yeh, M.; Brown, L. A. Airway Glutathione
479 Homeostasis is Altered in Children with Severe Asthma: Evidence for Oxidant Stress. *J. Allergy Clin.*
480 *Immunol.* **2009**, *123*, 146-152.
481 (28) Watson, W.; Ritzenthaler, J. D.; Roman, J. Lung Extracellular Matrix and Redox
482 Regulation. *Redox Biol.* **2016**, *8*, 303-315.
483 (29) Kinnula, V. L.; Fattman, C. L.; Tan, R. J.; Oury, T. D. Oxidative Stress in Pulmonary
484 Fibrosis: A Possible Role for Redox Modulatory Therapy. *Am. J. Respir. Crit. Care Med.* **2005**, *172*, 417-
485 422.
486 (30) Bakalova, R.; Zhelev, Z.; Aoki, I.; Saga, T. Tissue Redox Activity as a Hallmark of
487 Carcinogenesis: From Early to Terminal Stages of Cancer. *Clin. Cancer Res.* **2013**, *19*, 2503-2517.
488 (31) Kneller, J. M.; Lu, M.; Bracken, C. An Effective Method for the Discrimination of
489 Motional Anisotropy and Chemical Exchange. *J. Am. Chem. Soc.* **2002**, *124*, 1852-1853.
490 (32) Pantouris, G.; Syed, M. A.; Fan, C.; Rajasekaran, D.; Cho, T. Y.; Rosenberg, E. M., Jr.;
491 Bucala, R.; Bhandari, V.; Lolis, E. J. An Analysis of MIF Structural Features that Control Functional
492 Activation of CD74. *Chem Biol* **2015**, *22*, 1197-1205.
493 (33) Lubetsky, J. B.; Dios, A.; Han, J.; Aljabari, B.; Ruzsicska, B.; Mitchell, R.; Lolis, E.; Al-
494 Abed, Y. The tautomerase active site of macrophage migration inhibitory factor is a potential target for
495 discovery of novel anti-inflammatory agents. *J Biol Chem* **2002**, *277*, 24976-24982.
496 (34) Takahashi, K.; Koga, K.; Linge, H. M.; Zhang, Y.; Lin, X.; Metz, C. N.; Al-Abed, Y.;
497 Ojamaa, K.; Miller, E. J. Macrophage CD74 contributes to MIF-induced pulmonary inflammation. *Respir*
498 *Res* **2009**, *10*, 33.
499 (35) Mehrad, B.; Strieter, R. M.; Moore, T. A.; Tsai, W. C.; Lira, S. A.; Standiford, T. J. CXC
500 chemokine receptor-2 ligands are necessary components of neutrophil-mediated host defense in invasive
501 pulmonary aspergillosis. *J Immunol* **1999**, *163*, 6086-6094.
502 (36) Nguyen, M. T.; Beck, J.; Lue, H.; Funfzig, H.; Kleemann, R.; Koolwijk, P.; Kapurniotu,
503 A.; Bernhagen, J. A 16-residue peptide fragment of macrophage migration inhibitory factor, MIF-(50-65),
504 exhibits redox activity and has MIF-like biological functions. *J Biol Chem* **2003**, *278*, 33654-33671.

505 (37) Takahashi, M.; Nishihira, J.; Shimpo, M.; Mizue, Y.; Ueno, S.; Mano, H.; Kobayashi, E.;
506 Ikeda, U.; Shimada, K. Macrophage migration inhibitory factor as a redox-sensitive cytokine in cardiac
507 myocytes. *Cardiovasc Res* **2001**, *52*, 438-445.
508 (38) Pantouris, G.; Khurana, L.; Ma, A.; Skeens, E.; Reiss, K.; Batista, V. S.; Lisi, G. P.; Lolis,
509 E. J. Regulation of MIF Enzymatic Activity by an Allosteric Site at the Central Solvent Channel. *Cell*
510 *Chem Biol* **2020**, *27*, 740-750 e745.
511 (39) Calandra, T.; Roger, T. Macrophage migration inhibitory factor: a regulator of innate
512 immunity. *Nat Rev Immunol* **2003**, *3*, 791-800.
513 (40) Jung, H.; Seong, H. A.; Ha, H. Critical role of cysteine residue 81 of macrophage migration
514 inhibitory factor (MIF) in MIF-induced inhibition of p53 activity. *J Biol Chem* **2008**, *283*, 20383-20396.
515 (41) Filip, A. M.; Klug, J.; Cayli, S.; Frohlich, S.; Henke, T.; Lacher, P.; Eickhoff, R.; Bulau,
516 P.; Linder, M.; Carlsson-Skwirut, C.; Leng, L.; Bucala, R.; Kraemer, S.; Bernhagen, J.; Meinhardt, A.
517 Ribosomal protein S19 interacts with macrophage migration inhibitory factor and attenuates its pro-
518 inflammatory function. *J Biol Chem* **2009**, *284*, 7977-7985.
519 (42) Kassaar, O.; Pereira Morais, M.; Xu, S.; Adam, E. L.; Chamberlain, R. C.; Jenkins, B.;
520 James, T. D.; Francis, P. T.; Ward, S.; Williams, R. J.; van den Elsen, J. Macrophage Migration Inhibitory
521 Factor is subjected to glucose modification and oxidation in Alzheimer's Disease. *Sci Rep* **2017**, *7*, 42874.
522 (43) Maurice, M. M.; Nakamura, H.; van der Voort, E. A.; van Vliet, A. I.; Staal, F. J.; Tak, P.
523 P.; Breedveld, F. C.; Verweij, C. L. Evidence for the role of an altered redox state in hyporesponsiveness
524 of synovial T cells in rheumatoid arthritis. *J Immunol* **1997**, *158*, 1458-1465.
525 (44) Wu, S. M.; Pizzo, S. V. alpha(2)-Macroglobulin from rheumatoid arthritis synovial fluid:
526 functional analysis defines a role for oxidation in inflammation. *Arch Biochem Biophys* **2001**, *391*, 119-
527 126.
528 (45) Taylor, S. L.; Crawley-Snowdon, H.; Wagstaff, J. L.; Rowe, M. L.; Shepherd, M.;
529 Williamson, R. A.; Howard, M. J. Measuring protein reduction potentials using 15N HSQC NMR
530 spectroscopy. *Chem Commun (Camb)* **2013**, *49*, 1847-1849.
531 (46) Zimmermann, J.; Kuhne, R.; Sylvester, M.; Freund, C. Redox-regulated conformational
532 changes in an SH3 domain. *Biochemistry* **2007**, *46*, 6971-6977.
533 (47) Tjandra, N.; Feller, S. E.; Pastor, R. W.; Bax, A. Rotational diffusion anisotropy of human
534 ubiquitin from N-15 NMR relaxation. *J Am Chem Soc* **1995**, *117*, 12562-12566.
535 (48) Son, A.; Kato, N.; Horibe, T.; Matsuo, Y.; Mochizuki, M.; Mitsui, A.; Kawakami, K.;
536 Nakamura, H.; Yodoi, J. Direct Association of Thioredoxin-1 (TRX) with Macrophage Migration
537 Inhibitory Factor (MIF): Regulatory Role of TRX on MIF Internalization and Signaling *Antioxid. Redox*
538 *Signal.* **2009**, *11*, 2595-2605.
539 (49) Lubetsky, J. B.; Swope, M.; Dealwis, C.; Blake, P.; Lolis, E. Pro-1 of macrophage
540 migration inhibitory factor functions as a catalytic base in the phenylpyruvate tautomerase activity.
541 *Biochemistry* **1999**, *38*, 7346-7354.
542 (50) Zhong, F.; Lisi, G. P.; Collins, D. P.; Dawson, J. H.; Pletneva, E. V. Redox-dependent
543 stability, protonation, and reactivity of cysteine-bound heme proteins. *Proc Natl Acad Sci U S A* **2014**,
544 *111*, E306-315.
545 (51) Makhatadze, G. I.; Privalov, P. L. Heat capacity of proteins. I. Partial molar heat capacity
546 of individual amino acid residues in aqueous solution: hydration effect. *J Mol Biol* **1990**, *213*, 375-384.
547 (52) Privalov, P. L.; Makhatadze, G. I. Contribution of hydration and non-covalent interactions
548 to the heat capacity effect on protein unfolding. *J Mol Biol* **1992**, *224*, 715-723.
549 (53) Delaglio, F.; Grzesiek, S.; Vuister, G. W.; Zhu, G.; Pfeifer, J.; Bax, A. NMRPipe: a
550 multidimensional spectral processing system based on UNIX pipes. *J Biomol NMR* **1995**, *6*, 277-293.

551 (54) Lee, W.; Tonelli, M.; Markley, J. L. NMRFAM-SPARKY: enhanced software for
552 biomolecular NMR spectroscopy. *Bioinformatics* **2015**, *31*, 1325-1327.
553 (55) Loria, J. P.; Rance, M.; Palmer, A. G. A relaxation-compensated Carr-Purcell-Meiboom-
554 Gill sequence for characterizing chemical exchange by NMR spectroscopy. *J Am Chem Soc* **1999**, *121*,
555 2331-2332.
556 (56) Clore, G. M.; Szabo, A.; Bax, A.; Kay, L. E.; Driscoll, P. C.; Gronenborn, A. M. Deviations
557 from the Simple 2-Parameter Model-Free Approach to the Interpretation of N-15 Nuclear Magnetic-
558 Relaxation of Proteins. *J Am Chem Soc* **1990**, *112*, 4989-4991.
559 (57) Lipari, G.; Szabo, A. Model-Free Approach to the Interpretation of Nuclear Magnetic-
560 Resonance Relaxation in Macromolecules .2. Analysis of Experimental Results. *J Am Chem Soc* **1982**,
561 *104*, 4559-4570.
562 (58) d'Auvergne, E. J.; Gooley, P. R. Optimisation of NMR dynamic models I. Minimisation
563 algorithms and their performance within the model-free and Brownian rotational diffusion spaces. *J*
564 *Biomol NMR* **2008**, *40*, 107-119.
565 (59) d'Auvergne, E. J.; Gooley, P. R. Optimisation of NMR dynamic models II. A new
566 methodology for the dual optimisation of the model-free parameters and the Brownian rotational diffusion
567 tensor. *J Biomol NMR* **2008**, *40*, 121-133.
568 (60) MacLean, B.; Tomazela, D. M.; Shulman, N.; Chambers, M.; Finney, G. L.; Frewen, B.;
569 Kern, R.; Tabb, D. L.; Liebler, D. C.; MacCoss, M. J. Skyline: an open source document editor for creating
570 and analyzing targeted proteomics experiments. *Bioinformatics* **2010**, *26*, 966-968.
571